Turk J Elec Eng & Comp Sci, Vol.20, No.6, 2012, © TÜBİTAK
doi:10.3906/elk-1012-920

Vibration analysis of base structure on SINS using PZT actuators

Bin ZHENG[1], **Jianfeng YANG**[2,*]
[1]*School of Information and Communication Engineering, National Key Laboratory of Science and Technology on Electronic Test and Measurement, North University of China, Shanxi 030051, P.R. CHINA*
e-mail: zhengbin@nuc.edu.cn
[2]*School of Electronic Information, Soochow University, Jiangsu 215006, P.R. CHINA*
e-mail: jfyang@suda.edu.cn

Received: 21.12.2010

Abstract

A steel plate bonded with lead zirconate titanate (PZT) actuators was studied on the basis of finite element methods (FEMs). The damping amplitudes of this plate bonded with PZT actuators were obtained at different locations and under different control conditions by analyzing the distribution of the PZT plate's strain tensor in the first 4 modes. Furthermore, to reduce the unwanted disturbance and mitigate the errors from sensors, a base structure of the missile's strapdown inertial navigation system (SINS) is also proposed. The results show that the vibration control can be enhanced by increasing the number of the PZT actuators bonded. This implies that the application of the PZT actuators to the base of a missile's SINS is an effective approach for damping control.

Key Words: *Strapdown inertial navigation, PZT actuator, damping control, finite element methods*

1. Introduction

A strapdown inertial navigation system (SINS) makes the flight of a missile reliable and accurate. During the flight of missiles, harsh environments such as dynamic overload shock and angular vibration give rise to dynamic errors and impact flight stability and attitude control accuracy. Generally, in order to improve the accuracy of the SINS, Kalman filtering is used for its alignment and calibration [1,2]. Meanwhile, several methods to compensate for system errors on the moving base of missiles have been discussed in the literature [3]. Sanders et al. studied the vibration rectification error reducer for the fiber optic gyroscope of the SINS [4]. To satisfy the requirement of precise pointing in quiet environments, a variety of structural designs and control architectures, such as vibration isolation, can be applied [5]. The aim of this study is to explore methods to estimate and correct navigation errors and to improve the navigation accuracy of the SINS.

*Corresponding author: School of Electronic Information, Soochow University, Jiangsu 215006 P.R. CHINA

Vibration sensitivity can often be a dominant performance-limiting error source for the SINS. Plates and panels are primary structural components in the base of the SINS, and guidance accuracy is affected by platform vibration associated with the functioning of on-board equipment. In order to suppress excessive vibrations and improve system performance, additional passive damping treatment is usually not applicable. Therefore, increasing attention has been paid to active vibration control [6-8].

Some researchers [9] adopted a layerwise theory and an optimal control strategy to suppress the vibration of smart laminated beams. Wang et al. [10] established an accurate model for a composite smart beam with surface-bonded piezoelectric layers as actuators. In their study, a finite model was built based on the layerwise displacement theory and integrated electrical fields with mechanical properties.

With the development and the industrial realization of piezoelectric smart structures, finite element methods (FEMs) are widely applied in engineering fields because of their effective and reliable simulation [11-13]. Perry et al. [14] developed a finite element-based formulation for sensitivity analysis on piezoelectric media and simulated the sensitivity characteristics of a piezoelectric-based distributed mode actuator. Stanef et al. [15] calculated the resonance frequencies and mode shapes of both the structural and cavity modes using a finite element model. Kusculuoglu and Royston [16] proposed a FEM model for a piezoceramic laminated structure, which is applicable to both thick and thin plates. Belloli and Ermanni [17] established a computer-aided design model for the rear wing of a racing car and proposed a finite element model to investigate its optimum placement.

On the basis of the dynamic and transient response analysis of the plate and base structural model of the SINS, a simplified model for vibration control using lead zirconate titanate (PZT) actuators is studied here. Theoretically, the associated local flexural stiffening effects of the PZT actuators should also be taken into account. In this paper, the base structure of the SINS consists of several steel plates, and the flexural stiffening effects caused by the PZT actuators are much smaller compared to the effects caused by the steel plates. Therefore, they are neglected in this paper for simplicity. Moreover, the damping effects of different numbers and locations of the PZT actuators on the base structure of the SINS are also investigated through numerical simulation and experimental measurement.

Many studies have been carried on the vibration control of the soft Stewart platform and spacecraft [18,19], and the given natural frequency is 1.944 rad/s and less than 15 Hz. Comparing those to the results of previous studies, the structure frequency is higher in this paper, and the frequency of the 1st and 4th mode is 100.23 Hz and 1034 Hz, respectively. Thus, a larger control force should be adopted to reduce the vibration with the increasing stiffness in the paper. The vibration control using the PZT actuators can minimize the bulk of the SINS and improve the guidance accuracy during the missile's flight.

2. Finite element-based formulation for PZT base structure

This study focuses only on the base structure composed of several types of elastic materials as well as piezoelectric materials without any geometrical restriction, and only the elastic and PZT effects are taken into account. Under these conditions, the converse and direct PZT effects can be expressed as [20,21]:

$$\begin{cases} \sigma = c\varepsilon - eE \\ D = e^T\varepsilon + \Xi E \end{cases}, \tag{1}$$

where σ represents stress tensor, ε is the strain tensor, E denotes the electric field vector, D stands for the electric displacement vector, c stands for the elastic stiffness tensor at a constant electric field, e represents the

PZT stress tensor, and Ξ stands for the dielectric permittivity tensor at the constant strain.

The motion equation can be obtained using Hamilton's principle [22]:

$$\delta \int_{t1}^{t2} Ldt = \int_{t1}^{t2} (\delta T - \delta U + \delta W)dt = 0, \tag{2}$$

where $\delta U, \delta T$, and δW represent the variation of strain energy, the variation of kinetic energy, and the virtual work of applied forces, respectively.

$$T = \frac{1}{2} \int_{Vm} \rho_m \{\dot{r}\}^T \{\dot{r}\} dv + \frac{1}{2} \int_{Vp} \rho_p \{\dot{r}\}^T \{\dot{r}\} dV, \tag{3}$$

$$U = \frac{1}{2} \int_{Vm} \{\varepsilon\}^T \{\sigma\} dV + \frac{1}{2} \int_{Vp} \{\varepsilon\}^T \{\sigma\} dV - \frac{1}{2} \int_{Vp} \{E\}^T \{D\} dV, \tag{4}$$

$$W = \int_{S1} \{r\}^T \{f_s\} dS + \{r\}^T \{f_c\} - \int_{S2} \{Q\}^T \{O^e\} dS, \tag{5}$$

where $\{r\} = [N_r]\{r^e\}$ represents the displacement vector, ρ_m and ρ_p respectively stand for the material densities of the main structure and piezoelectric material, $\{E\}$ represents the electric field vector, $\{D\}$ is the electric displacement vector, $\{f_s\}$ denotes the surface force applied to surface S_1, $\{O^e\}$ is the charge density applied to surface S_2, and $\{f_c\}$ is the external force.

According to [9] and [23], the element motion equation and the output voltage of the sensor can be written as:

$$[m]\{r^e\} + [k_{QQ}]\{Q^e\} = \{f\} + \{g\}, \tag{6}$$

$$\{V\} = \{Q\} = -[k_{QQ}]^{-1}[k_{Qr}]\{r\}. \tag{7}$$

3. Results and discussion

The PZT-plate element was validated for sensing and actuation performance. The study on vibration control was conducted on a steel plate with dimensions of 0.23 m × 0.1 m × 0.002 m. The piezoelectric properties of the PZT actuator are shown in Table 1. The cantilever plate is clamped at one end, and the excitation force F_y is imposed on the other free end.

Table 1. Properties of the piezoelectric materials and basic steel materials.

Properties	Piezoelectric material	Steel
Young's modulus, E (N/m^2)	63.0×10^9	200×10^9
Density, ρ (kg/m^3)	7600.0	7800.0
Poisson's ratio, ν	0.30	0.34
Piezoelectric strain constant, d_{31} (10^{-12} C/N)	–274	-
Piezoelectric strain constant, d_{33} (10^{-12} C/N)	593	-

The vibration characteristics of the plate bonded with PZT sensors and actuators were analyzed with the FEM software ANSYS. Figures 1a, 1b, 1c, and 1d show the bending and torsion of the plate structure in the first 4 modes from the numerical results, where the frequencies of the plate are at 31.515 Hz, 151.30 Hz, 194.4 Hz, and 482.87 Hz, respectively.

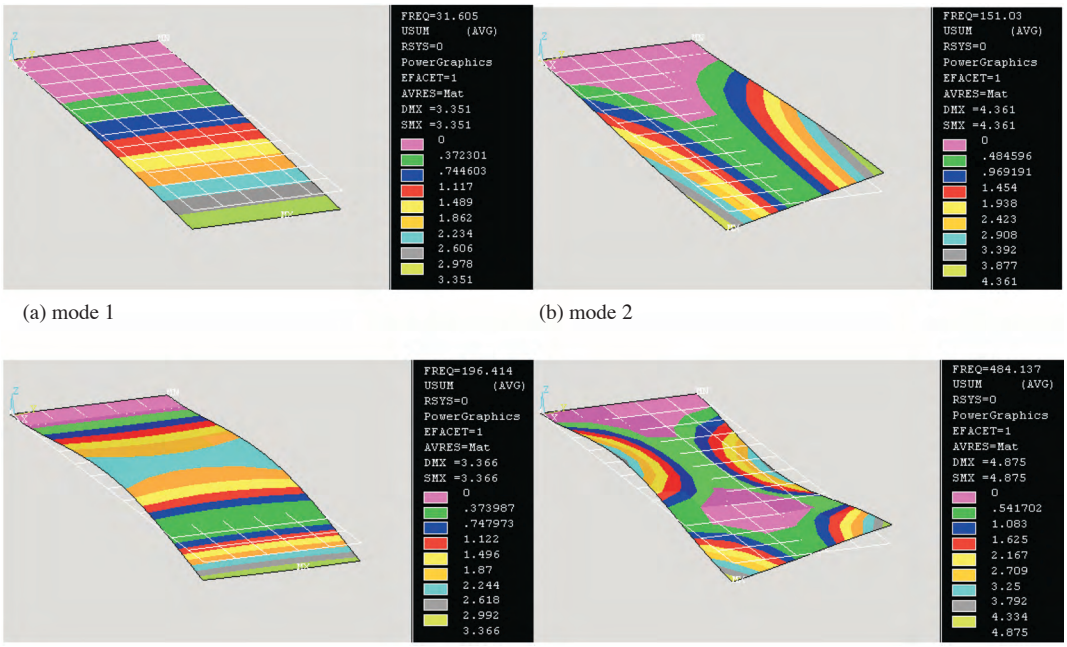

(a) mode 1 (b) mode 2

(c) mode 3 (d) mode 4

Figure 1. The first 4 modes of the plate structure: a) the 1st mode, bending in the X and Z plane (31.515 Hz), b) the 2nd mode, torsion in the X and Y plane (151.30 Hz), c) the 3rd mode, bending in the X and Z plane (194.4 Hz), and d) the 4th mode, torsion in the X and Y plane (482.87 Hz).

The plate in Figure 2 is partitioned 5 $\times$ 12 into a total of 60 elements and the size of each element is 19.17 mm $\times$ 20 mm. The sizes of the PZT actuators are the same as those of the plate elements. The distribution of the strain tensor ε in the 1st mode using 5 $\times$ 12 elements is illustrated in Figure 3. The largest strain tensor is at the center on the fixed end.

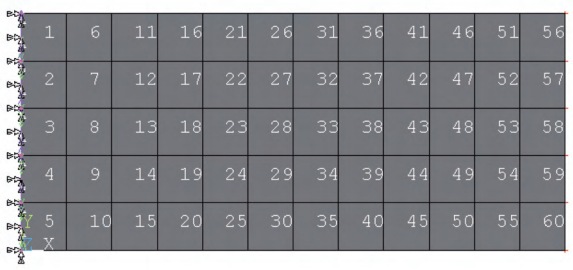

Figure 2. The distribution of the plate with 5 $\times$ 12 elements.

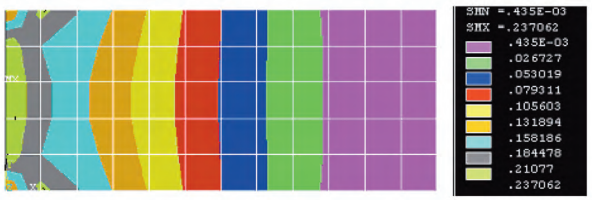

Figure 3. Distribution of strain tensor ϵ in the 1st mode.

According to the distribution of the strain tensor, the PZT actuators are placed at different locations for damping control. The control voltage of the PZT actuators is selected along the change of the excitation force at the free end.

In order to suppress the vibration amplitude of the plate structure, the PZT actuators should be bonded on the location of each element. The damping amplitude under different control conditions of C1, C2, C3, and C4 is shown in Figure 4, which represents different control locations and the quantities of the PZT actuators on the plate structure, where m is meter for length. As the numbers of the PZT actuators increase, the vibration amplitude decreases. Figure 4 illustrates the damping ratio with the distributed control force $F = -1\cos\omega t$ caused by the PZT actuators and the excited force, $F_y = -1\cos\omega t$, at the free end. The damping ratio is 23.8%, 35.5%, and 68.3% with respect to the free system (C1), respectively. Similarly, the damping amplitude under different control conditions, i.e. with the control force and the excited force changed to $F = F_y = -2\cos\omega t$ and $F = F_y = -5\cos\omega t$, is shown in Figures 5 and 6.

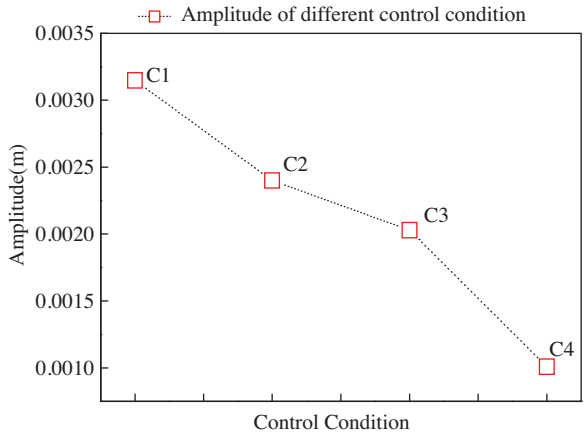

Figure 4. Amplitude under different control conditions: C1, uncontrolled; C2, controlled at locations 2-4; C3, controlled at locations 1-5; C4, controlled at locations 1-10; $F = F_y = -1\cos\omega t$.

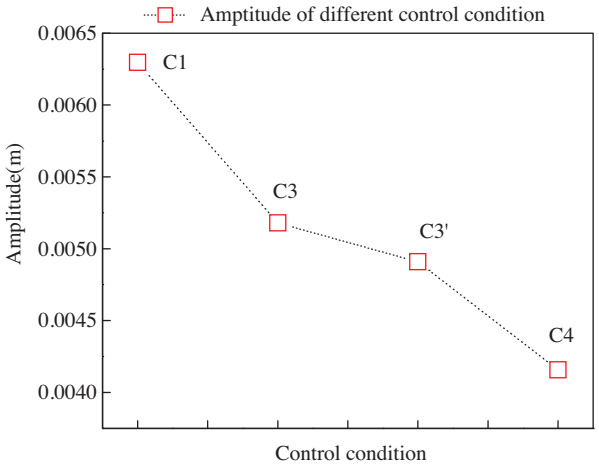

Figure 5. Amplitude under different control conditions: C1, uncontrolled; C3, controlled at locations 1-5; C3', controlled at locations 1-5 and 8; C4, controlled at locations 1-10; $F = F_y = -2\cos\omega t$.

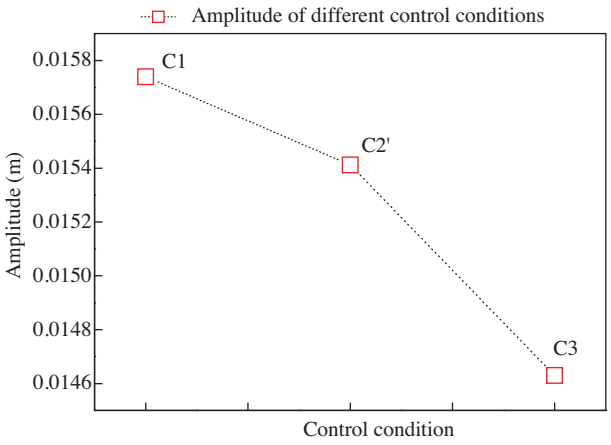

Figure 6. Amplitude under different control conditions: C1, uncontrolled; C2', controlled at location 3; C3, controlled at locations 1-5; $F = F_y = -5\cos\omega t$.

In Figures 4-6, with an increase in the excited force, the damped amplitude becomes larger. Meanwhile, the damping ratio becomes smaller under the same control force by the same number of PZT actuators.

The same plate in Figure 2 is divided into 8 × 8 elements and the size of each PZT actuator is 28.75 mm × 12.5 mm. The distribution of the strain tensor ϵ in the 1st mode using 8 × 8 elements is depicted in Figures 7 and 8. Similar to that of Figure 3, the largest strain tensor is close to the fixed end.

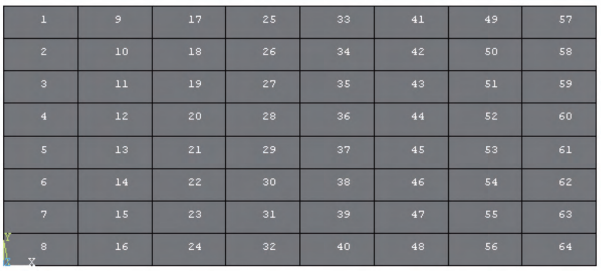

Figure 7. The distribution of the plate with 8 × 8 elements.

Figure 8. Distribution of strain tensor ϵ in the 1st mode with 8 × 8 elements.

Similar damping amplitudes under different control conditions are shown in Figures 9-11. The control force is $F = F_y = -1\cos\omega t$ and the excited force is $F = F_y = -2\cos\omega t$ and $F = F_y = -5\cos\omega t$, respectively.

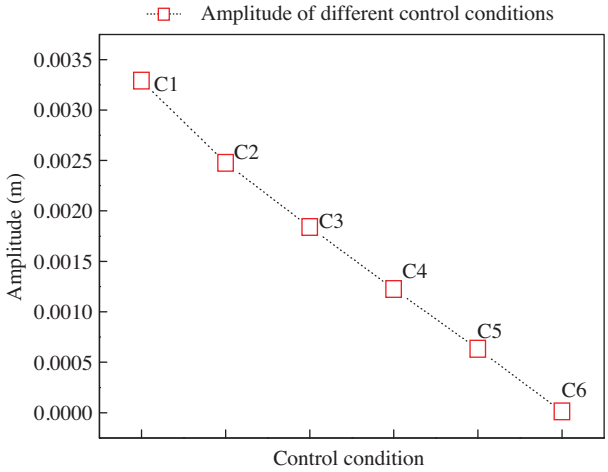

Figure 9. Amplitude under different control conditions: C1, uncontrolled; C2, controlled at locations 4 and 5; C3, controlled at locations 3-6; C4, controlled at locations 2-7; C5, controlled at locations 1-8; C6, controlled at locations 1-8, 12, and 13; $F = F_y = -1\cos\omega t$.

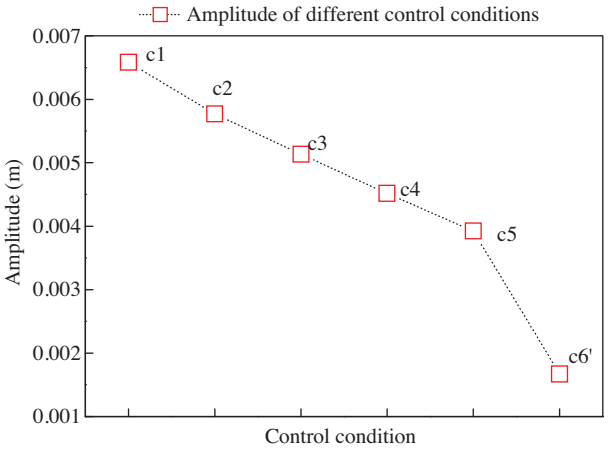

Figure 10. Amplitude under different control conditions: C1, uncontrolled; C2, controlled at locations 4 and 5; C3, controlled at locations 3-6; C4, controlled at locations 2-7; C5, controlled at locations 1-8; C6', controlled at locations 1-16; $F = F_y = -2\cos\omega t$.

From the results of 2 different element sizes in Figures 2 and 7, the control effect is related to the quantities of PZT actuators. With an increase in the numbers of PZT actuators, the damping ratio of the plate structure can be reduced clearly. It is concluded that the 2nd case (8 × 8) leads to higher control accuracy than the 1st (5 × 12) because of the increasing of element numbers under the same plate. Moreover, during the vibration control experiment, the plate can be partitioned into a certain size with the requirement of the PZT actuators' size in the practical application.

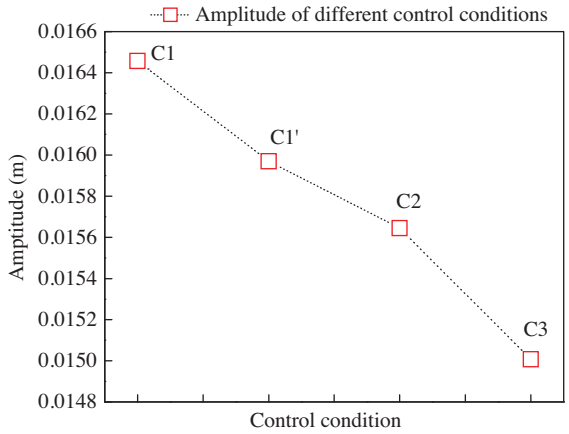

Figure 11. Amplitude under different control conditions: C1, uncontrolled; C1', controlled at location 5; C2, controlled at locations 4 and 5; C3, controlled at locations 3-6; $F = F_y = -5\cos\omega t$.

From the results of 2 different element sizes in Figures 2 and 7, the control effect is related to the quantities of PZT actuators. With an increase in the numbers of PZT actuators, the damping ratio of the plate structure can be reduced clearly. It is concluded that the 2nd case (8×8) leads to higher control accuracy than the 1st (5×12) because of the increasing of element numbers under the same plate. Moreover, during the vibration control experiment, the plate can be partitioned into a certain size with the requirement of the PZT actuators' size in the practical application.

Inertial elements of the SINS, such as the gyroscope and accelerometer, are fixed on the base without opposite movement. Navigation precision is dependent on dynamic errors, impulse, and angle vibration of the inertial element. To enhance system precision, the vibration of the SINS should be under real-time track-based control. Vibration control of the SINS using piezoelectric materials was also studied based on our research of the plate structure.

The SINS position and the coordinates of the missile flight are shown in Figure 12, where X and Z represent the radial axis and Y stands for the actual flying direction of the missile. The constraint and boundary of the SINS are also described in Figure 12. The simulation results of the vibration mode of the SINS using ANSYS software are listed in Table 2.

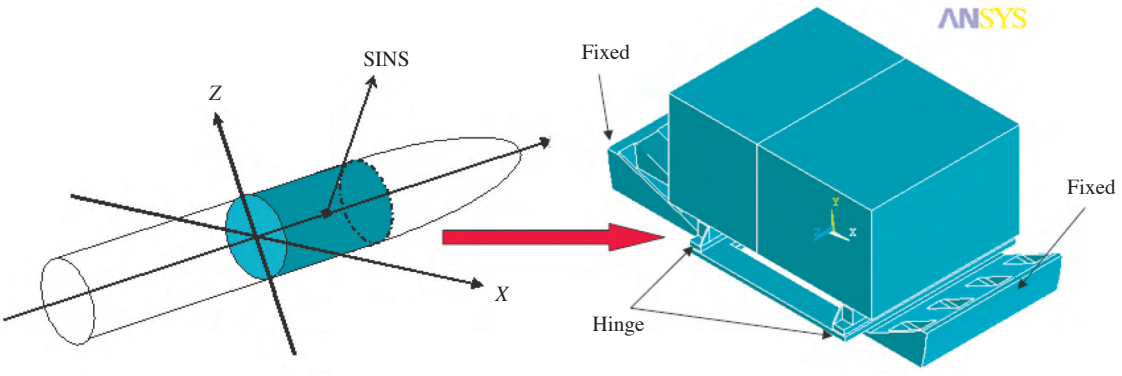

Figure 12. The SINS position on the missile and the constraint and boundary of the SINS.

In Figure 13, the 1st and the 4th modes represent the torsions in the X and Z axis, respectively. Since these torsions are along the radial axis, they have minor influence on precision control. The 2nd and the 3rd

modes represent the bending in the X and Y axis, respectively. Since the missile flight is in the Y direction, the bending in the Y axis has significant impact on precision control. Therefore, this study focuses on the 2nd and 3rd modes.

Table 2. Simulation results of the vibration modes.

Modes	f / Hz	Status
The 1st mode	100.23	Torsion in the Xaxis
The 2nd mode	235.45	Bend in the XY area
The 3rd mode	282.98	Bend in the XY area
The 4th mode	1034	Torsion in the Yaxis

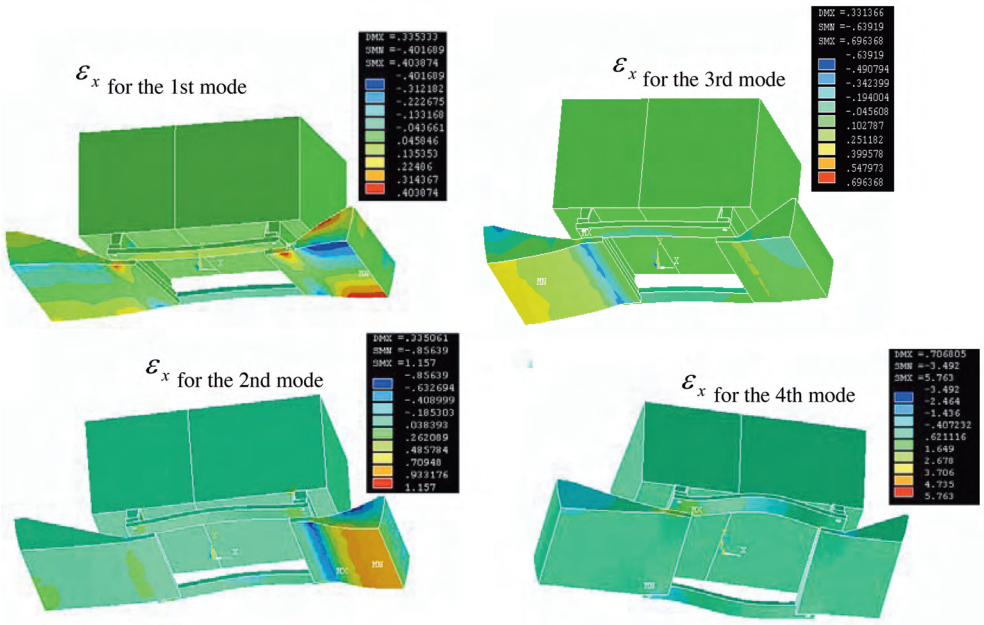

Figure 13. Distribution of strain tensor ε_x in the different modes.

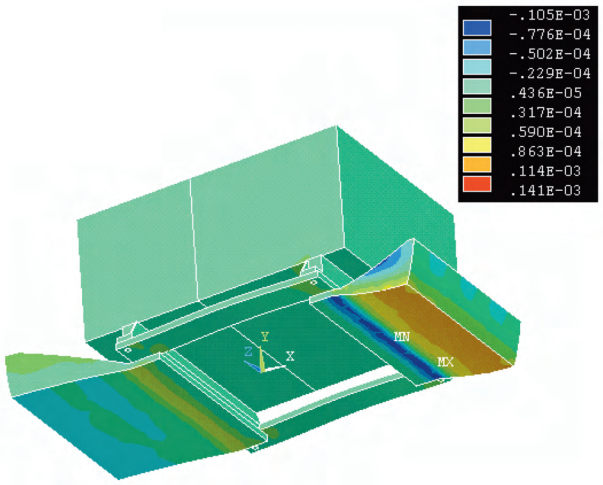

Figure 14. Distribution of strain tensor o ε under forced vibration in the 2nd mode.

A cruise missile with an acceleration of 20 g in the Y axis has a great impact on precision control. The force (96 N) imposed on 2 flanks of the brackets is adopted in the simulation. In the 2nd mode, the location of the maximum deformation remains the same under free and forced vibration conditions, and it is at the junction between the base structure and the SINS bonded with piezoelectric material. The PZT actuator can be bonded on the structural base of the SINS for vibration control. Considering the large stiffness of the inertial navigation system, large piezoelectric material (40 mm $\times$ 20 mm $\times$ 0.5 mm) is selected. The location of the piezoelectric material, with the control force of $F_y = -96\cos\omega t$, bonded onto the base structure of the SINS is shown in Figure 15.

Under different control conditions, different damping amplitudes can be obtained from the simulation on the base structure of the SINS model in Figure 16. The excitation force is at the middle of the base.

When the structure base is uncontrolled, the vibration amplitude is 0.44545×10^{-4} m. Once a PZT actuator is bonded with the base, the vibration amplitude can be suppressed to 0.389282×10^{-4} m. From conditions C1 to C4, the damping rates are 12.6%, 23.4%, and 31.47% with respect to the control-free system (C1), respectively. As the quantities of the PZT actuator increase, control efficiency is improved.

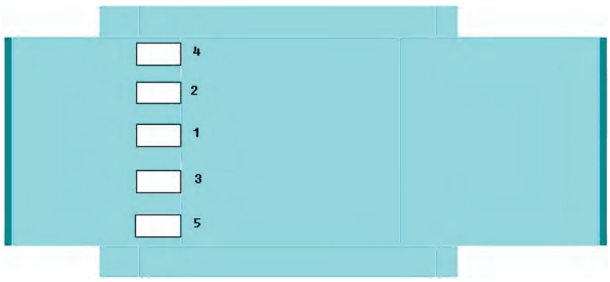

Figure 15. PZT actuators bonded onto the base of the SINS model.

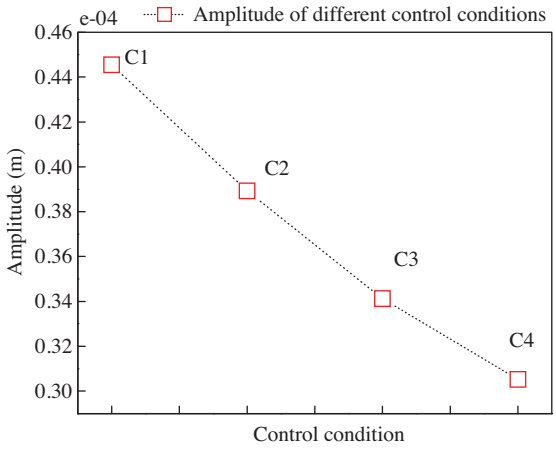

Figure 16. Amplitude under different control conditions: C1, uncontrolled; C2, controlled at location 1; C3, controlled at locations 1-3; C4, controlled at locations 1-5; $F = 235Hz$ and $F_y = -96\cos\omega t$.

To validate the proposed method in this paper, a comparison between the theoretical and experimental studies on the simplified base structural of the SINS system (seen in Figure 15) was performed. The damping results (seen in Figure 17) of the system were obtained by numerical calculations on a steel plate. The 3 curves in Figure 17 illustrate the damping results of the system for uncontrolled conditions, with 1 PZT actuator, and with 2 PZT actuators, respectively. The numerical results for the 3 different control conditions in Figure 17 demonstrate that the damping amplitude can be lowered by increasing the number of actuators. With the increase of the actuators, the system can be stabilized quickly due to the increased damping.

To obtain the damping logarithmic decrement, the damping amplitudes at the extremities are illustrated in Figure 18. Detailed analysis in Figure 18 shows that the logarithmic decrement is 0.035, 0.29, and 0.65, respectively.

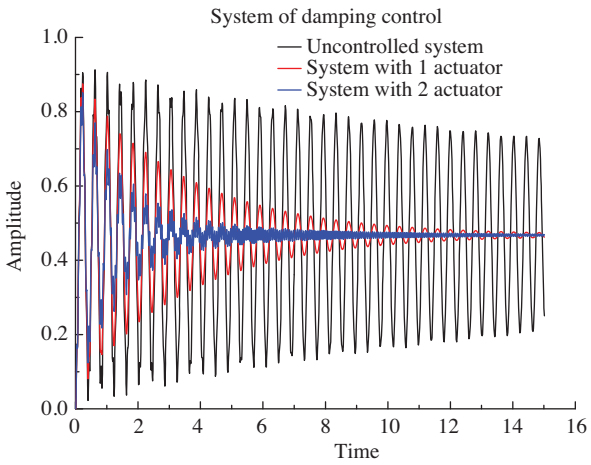

Figure 17. The system of damping control using numerical simulation.

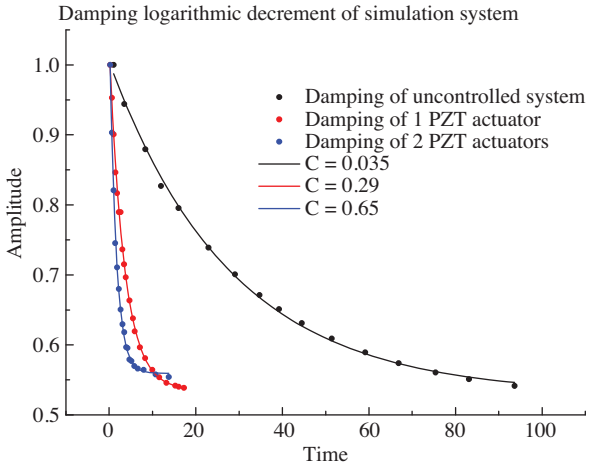

Figure 18. The damping logarithmic decrement of the simulation system.

As a comparison, the experimental results are given in the following Figures. Damping amplitudes as a function of time for the above 3 control conditions are shown in Figure 19. The impulse response of the system is detected by an analog-to-digital converter using 3 different control methods, which are uncontrolled, 1 PZT actuator control and 2 PZT actuator controls, respectively. In Figure 19, during the time period from 4.2 s to 11.5 s, the system is controlled with the structure composed of the steel material; from 15 s to 17.5 s, the system is controlled using 1 PZT actuator control; and from 21.0 s to 23.0 s, the system is controlled using 2 PZT actuator controls. The comparison of the 3 different control methods shows that the system has the best stability when using 2 PZT actuator controls.

Corresponding to the results in Figure 19, the experimental damping logarithmic decrement results of the different control systems are illustrated in Figure 20. The damping coefficient of the uncontrolled system is shown using the black line, where C = 0.029. The damping logarithmic decrements of the control systems with 1 PZT actuator and 2 PZT actuators are 0.22 and 0.35, respectively. As the number of PZT controllers increases, the stability and the damping logarithmic decrement of the system are also increased.

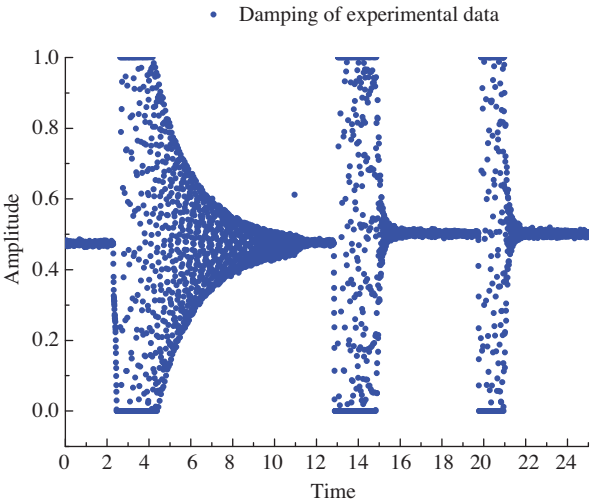

Figure 19. The system of damping control using the experimental data.

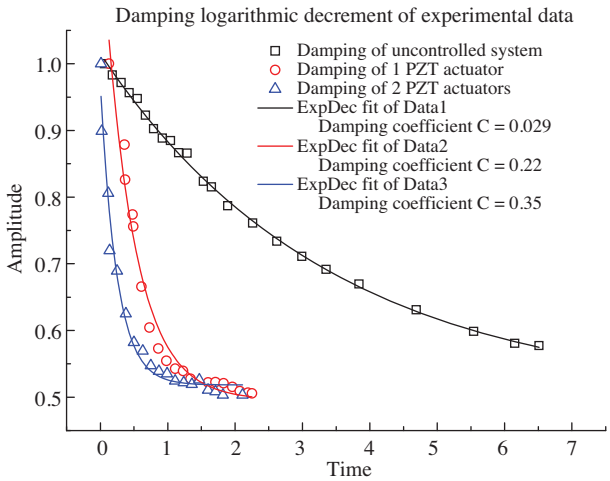

Figure 20. The damping logarithmic decrement of the experimental data.

Figure 21 shows the comparison of the frequency responses for the 3 different control methods; we can see that the amplitude of the frequency response decreases when the system uses more PZT actuators at 32.8 Hz. From the inset of Figure 21, the different frequency responses for the 3 control methods are shown clearly, where the maximum amplitudes of the frequency response are suppressed from 0.62 and 0.42 to 0.28 at the frequency of 32.8 Hz.

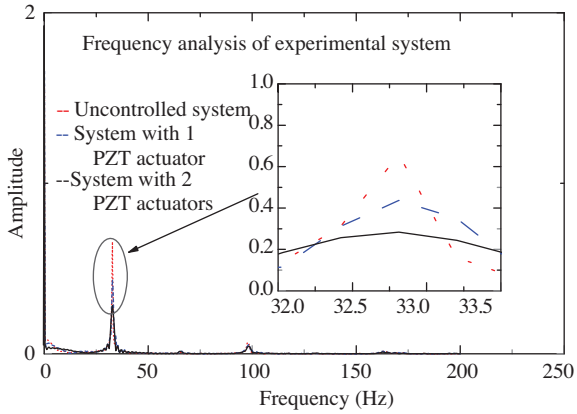

Figure 21. Frequency analysis of the experimental system.

The curves of time-amplitude and frequency-amplitude are shown in Figures 20 and 21. From the experimental results of the damping logarithmic decrement and frequency spectrum, the validation of vibration control on a thick steel plate is approved, and better control effectiveness using 2 PZT actuators is verified.

4. Conclusion

A study on a steel plate bonded with PZT actuators using the FEM was conducted. The distribution of the PZT plate's strain tensor in the first 4 modes was analyzed using ANSYS software, and the damping amplitudes of the plate bonded with PZT actuators at different locations and under different control conditions were calculated. Moreover, the missile's SINS with the base bonded with PZT actuators for vibration control was also proposed. The simulation demonstrated that the precision of the vibration control can be improved by increasing the number of PZT actuators.

The SINS with relatively larger stiffness and higher frequency was also studied. This is helpful to minimize the structure of the SINS and increase the difficulties for missile defense. Moreover, the errors caused by the vibration effects on the system can be reduced, and this leads to higher accuracy of an inertial navigation system. This implies that the application of the PZT actuator to the missile SINS base is an effective way for damping control.

References

[1] F. Xu, J.C. Fang. "Velocity and position error compensation using strapdown inertial navigation system/celestial navigation system integration based on ensemble neural network", Aerospace Science and Technology, Vol. 12, pp. 302-307, 2008.

[2] J. Ali, J.C. Fang. "SINS/ANS integration for augmented performance navigation solution using unscented Kalman filtering", Aerospace Science and Technology, Vol. 10. pp. 233-238, 2006.

[3] X Wang, L Guo. "An intelligentized and fast calibration method of SINS on moving base for missiles", Aerospace Science and Technology, Vol. 13, pp. 216-223, 2009.

[4] G.A. Sanders, R.C. Dankwort, A.W. Kaliszek, C.E. Laskoskie, L.K. Strandjord, D.L. Sugarbaker, J.L. Page, Vibration Rectification Error Reducer for Fiber Optic Gyroscope, United States Patent 5,946,097, 1999.

[5] G.S. Hanuge, M.E. Campbell, "Sensors and control of a space-based six-axis vibration isolation system", Journal of Sound and Vibration, Vol. 269, pp. 913-931, 2004.

[6] T. Chen, C. Hu, W.H. Huang. "Vibration control of cantilevered Mindlin-type plates", Journal of Sound and Vibration, Vol. 320, pp. 221-234, 2009.

[7] M.K. Kwak, S. Heo, M. Jeong. "Dynamic modeling and active vibration controller design for a cylindrical shell equipped with piezoelectric sensors and actuators", Journal of Sound and Vibration, Vol. 321, pp. 510-524, 2009.

[8] C.D. Marqui Jr, A. Erturk, D.J. Inman. "An electromechanical finite element model for piezoelectric energy harvester plates", Journal of Sound and Vibration. Vol. 327, pp. 9-25, 2009.

[9] A. Zabihollah, R. Sedagahti, R. Ganesan. "Active vibration suppression of smart laminated beams using layerwise theory and an optimal control strategy", Smart Material and Structures, Vol. 16, pp. 2190-2201, 2007.

[10] F. Wang, G.J. Tang, D.K. Li. "Accurate modeling of a piezoelectric composite beam", Smart Material and Structures, Vol. 16, pp. 1595-1602, 2007.

[11] J. Becker, O. Fein, M. Maess, L. Gaul. "Finite element-based analysis of shunted piezoelectric structures for vibration damping", Computers and Structures, Vol. 84, pp. 2340-2350, 2006.

[12] A.E.V. do Espirito Santo, M.R. Calado, C.M.P. Cabrita. "Design and evaluation of a linear switched reluctance actuator for positioning tasks", Turkish Journal of Electrical Engineering & Computer Sciences, Vol. 18, pp. 925-941, 2010.

[13] Ö. Özgün, M. Kuzuoğlu, "Recent advances in perfectly matched layers in finite element applications", Turkish Journal of Electrical Engineering & Computer Sciences, Vol. 16, pp. 57-66, 2008.

[14] M.A. Perry, R.A. Bates, M.A. Atherton, H.P. Wynn. "A finite-element-based formulation for sensitivity studies of piezoelectric systems", Smart Material and Structures, Vol. 17, pp. 1-7, 2008.

[15] D.A. Stanef, C.H. Hansen, R.C. Morgans. "Active control analysis of mining vehicle cabin nosing using finite element modeling", Journal of Sound and Vibration, 277, pp. 277-297, 2004.

[16] Z.K. Kusculuoglu, T.J. Royston. "Finite element formulation for composite plates with piezoceramic layers for optimal vibration control applications", Smart Material and Structures, Vol. 14, pp. 1139-1153, 2005.

[17] A. Belloli, P. Ermanni. "Optimum placement of piezoelectric ceramic modules for vibration suppression of highly constrained structures", Smart Material and Structures, Vol. 16, pp. 1662-1671, 2007.

[18] A. Kumar, J.L. Crassidis, "Colored-noise Kalman filter for vibration mitigation of position/attitude estimation systems", AIAA Guidance, Navigation and Control Conference and Exhibit, AIAA Paper #2007-6516, 2007.

[19] D. Kamesh, R. Pandiyan, A. Ghosal, "Modeling, design and analysis of lower frequency platform for attenuating micro-vibration in spacecraft", Journal of Sound and Vibration, Vol. 329, pp. 3431-3450, 2010.

[20] S.X. Xu, T.S. Koko, "Finite element analysis and design of actively controlled piezoelectric smart structures", Finite Elements in Analysis and Design, Vol. 40, pp. 241-262, 2004.

[21] F. Cote, P. Masson, N. Mrad, V. Cotoni, "Dynamic and static modeling of piezoelectric composite structures using a thermal analogy with MSC/NASTRAN", Composite Structures, Vol. 65, pp. 471-484, 2004.

[22] I.G. Lim, I. Lee. "Aeroelastic analysis of bearingless rotors with a composite flexbeam", Composite Structures, Vol. 88, pp. 570-578, 2009.

[23] S.H. Chen, Z.D. Wang, X.H. Liu. "Active vibration control and suppression for intelligent structures", Journal of Sound and Vibration, Vol. 200, pp. 167-177, 1997.